–Title of my thesis–

Shreeprasad Bhat

A Thesis Submitted to

Indian Institute of Technology Hyderabad

In Partial Fulfillment of the Requirements for

The Degree of Master of Technology

Department of Artificial Intelligence

June 2022

Declaration

I declare that this written submission represents my ideas in my own words, and where ideas or words of others have been included, I have adequately cited and referenced the original sources. I also declare that I have adhered to all principles of academic honesty and integrity and have not misrepresented or fabricated or falsified any idea/data/fact/source in my submission. I understand that any violation of the above will be a cause for disciplinary action by the Institute and can also evoke penal action from the sources that have thus not been properly cited, or from whom proper permission has not been taken when needed.

_____

(Signature)

_____

(Shreeprasad Bhat)

_____

(Roll No.)

Approval Sheet

This Thesis entitled –Title of my thesis– by Shreeprasad Bhat is approved for the degree of Master of Technology from IIT Hyderabad

---

(———-) Examiner
Dept. of Chem Eng
IITH

(———-) Examiner
Dept. Math
IITH

(Dr. Shantanu Desai) Adviser
Dept. of Physics
IITH

(———) Chairman
Dept. of Artificial Intelligence
IITH

Abstract

This is not a document on how to use latex. It rather explains how to use iiththesis.cls file to write your thesis for PhD/M.Tech/MSc. This file is generated using the class iiththesis.cls. This document draws a broad picture of the structure and formatting of your thesis.

Contents

Chapter 1

Model-independently calibrating the luminosity correlations of GRBs using deep learning

1.1 Introduction

The accelerating expansion of the universe is first found from the fact that the luminosity of type Ia supernovae (SNe Ia) is dimmer than expected [1]. This led to the discovery of Dark energy [2]. One of the few ways to measure properties of dark energy is to extend the Hubble Diagram(HD) to high redshift. The only way to extend HD to higher redshift is to Gamma Ray Burts (GRB). GRB have been found to be reasonably good standard candles in the usual sense that light curve and/or spectral properties are correlated to the luminosity, exactly as for Cepheids and supernovae, then simple measurements can be used to infer their luminosities and hence distances. The default expectation is the simplest model for the Dark Energy, where it does not change in time. This can be parametrized with the equation of state of the Dark Energy. The concordance case has w = -1 at all times, and this is the expectation of Einstein's cosmological constant, or if the Dark Energy arises from vacuum energy. Given the strong results from supernovae for redshifts of less than 1, the frontier has now been pushed to asking the question of whether the value of w changes with time (and redshift).

The best way to measure properties of the Dark Energy seems to be to measure the expansion history of our Universe and place significant constraints on models of the Universe. Hubble diagram can be used to measure it. The Hubble diagram (HD) is a plot of distance versus redshift, with the slope giving the expansion history of our Universe. been proposed to determine the distances and redshifts of two thousand supernovae per year out to redshift 1.7 with exquisite accuracy. The default expectation is the simplest model for the Dark Energy, where it does not change in time. This can be parameterized with the equation of state of the Dark Energy. The best way to measure whether dark energy changed with respect to redshift, is to measure it over wide range of redshifts, but supernovaes cannot be deteceted above 1.7 even with modern satelites. But GRBs offer means extend HD over redshift > 6. The reason is that GRBs are visible across much larger distances than

supernovae.

GRBs are now known to have several light curve and spectral properties from which the luminosity of the burst can be calculated (once calibrated), and these make GRBs into 'standard candles'.

1.2 Literature Survey

The first work on luminosity correlation of GRBs was done by [3]. [4] shows that not all luminosity correlations are applicable across all redshifts. [5] prooves otherwise. [6] shows that is not true. [7] have model independetently verified this using deep learning.

1.3 Observational Data

1.3.1 GRB

The GRB dataset we use is from [6]. In Table 1, we list the variables of 116 GRBs that we use in fitting luminosity correlations

1.3.2 Pantheon

Pantheon compilation [8] is the combined sample of SNe Ia discovered from different surveys to form the largest sample consisting of total of 1048 SNe Ia raning from $0.01 < z < 2.3$.

1.3.3 Union

The updated supernova Union2.1[9] compilation of 580 SNe is available at http://supernova.lbl.gov/Union

1.4 Methodology

1.4.1 Gaussian Processes

1.4.2 Reccurent Neural Networks

to be written...

1.5 Reconstruction and calibration of distance modulus using Gaussian Processes

We first use Gaussian processes to reconstruct $\mu - z$ relation from pantheon data. Gaussian processes can construct function without involving any model assumption. The Gaussian processes only depend on the covariance function $k(x, x')$, which characterizes the correlation between the function value at x to that at x'. There are many covariance functions available, but any covariance function

should be positive definite and monotonously decreasing with the increment of distance between x and x'. Here we use the following kernel

$$k(x, x') = ConstantKernel() + 1.0 * DotProduct(1) * *0.1 + 1.0 * WhiteKernel(1) \tag{1.1}$$

Our kernel (1.1) is a sum of linear, constant and whitekernels. Linear Kernel with exponent is used to capture relation in the data, constant kernel is used as scale magnitude and white kernel explains the noise in the input.

1.5.1 Training

We optimize the hyper-parameters of kernels by maximizing the marginal likelihood marginalized over function values f at the whole locations X. We use the publicly available python package sklearn[10] to reconstruct distance modulus as a function of redshift. The results are plotted in (1.2). The posterior samples drawn from kernel is shown in (1.1) .In the range where data points are sparse, the uncertainty of the reconstructed function is large. While training GP numerical issues are common to occur, hence we set $\alpha = 0.3$ and standardize the distance modulus before training. We also restart optimizer 100 times, parameters sampled log-uniform randomly from the space of allowed range.

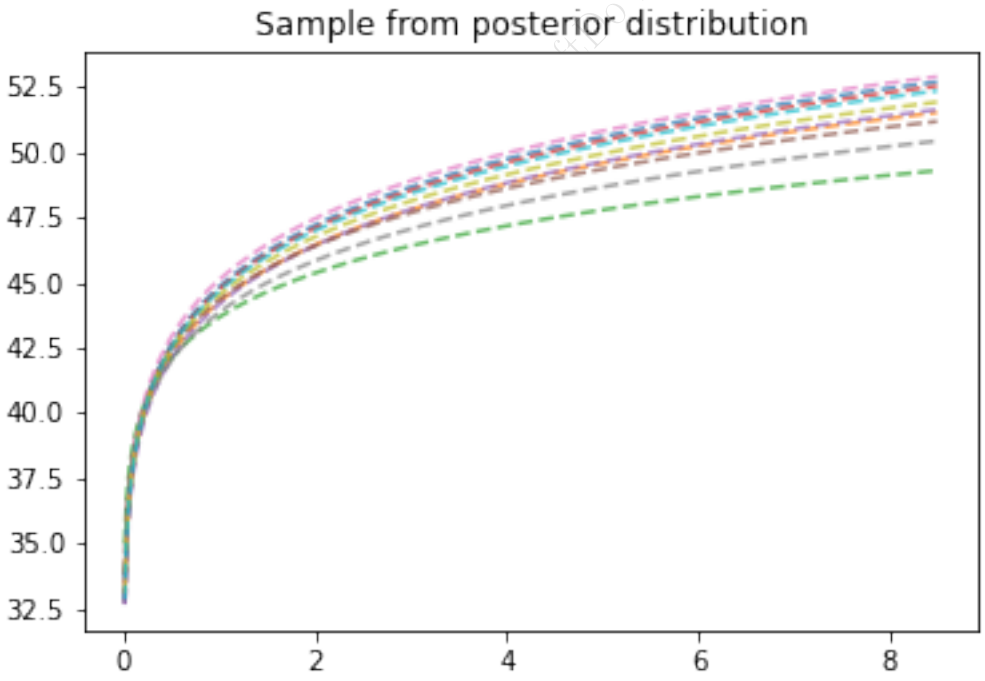

Figure 1.1: Posterior samples drawn from GP

The error bars with predictions are shown below
Log Marginal Likelihood = -20.3
The coefficient of determination R^2 = 0.9951

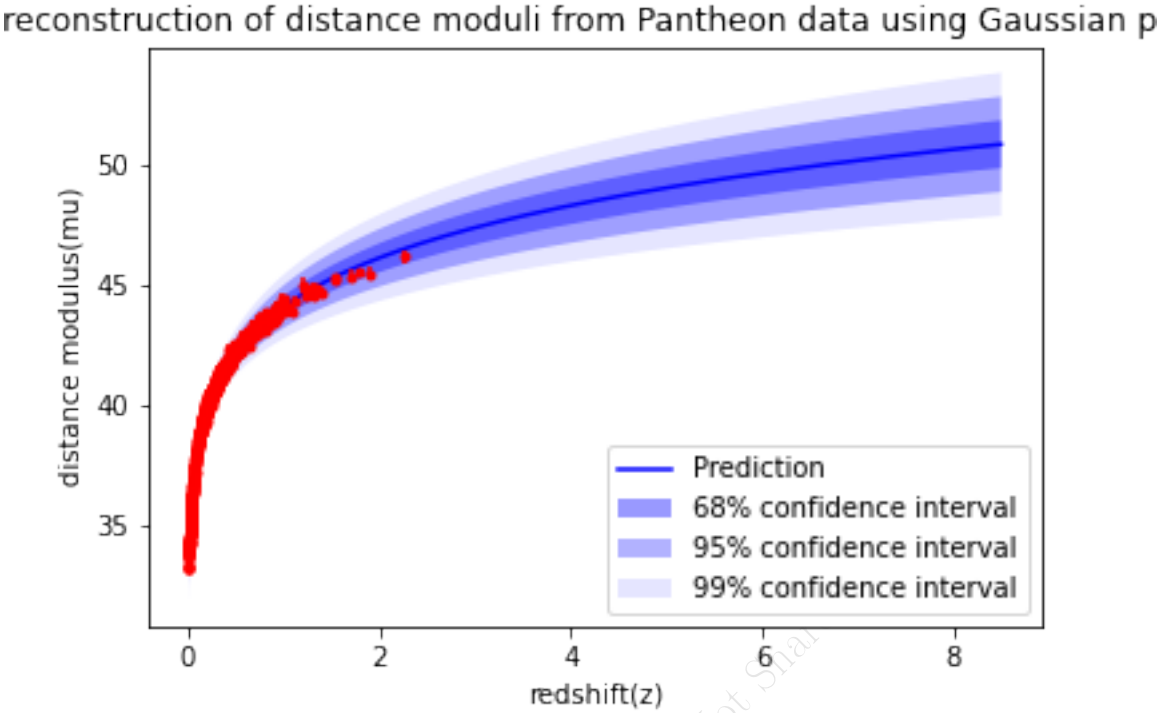

Figure 1.2: The reconstruction of distance moduli from Pantheon data set using GP. The red dots with 1σ error bars are the Pantheon data points. The light-blue dots are the central values of reconstruction. The shaded regions are the 1σ, 2σ and 3σ uncertainties.

1.5.2 Testing redshift dependence of luminosity correlations

The luminosity relations are connections between measurable parameters of the light curves and/or spectra with the GRB luminosity. Specifically, I will be using the power law relationships between explained below. This section will discuss the calibration of all six relations. The calibration will essentially be a fit on a log-log plot of the luminosity indicator versus the luminosity. For this calibration process, the burst's luminosity distance must be known to convert Pbolo to L (or Sbolo to Egamma) and this is known only for bursts with measured redshifts. However, an important point is that the conversion from the observed redshift to a luminosity distance is done by machine learning model. The observed luminosity indicators will have different values from those that would be observed in the rest frame of the GRB. That is, the light curves and spectra seen by Earth-orbiting satellites suffer time-dilation and redshift. The physical connection between the indicators and the luminosity is in the GRB rest frame, so we must take our observed indicators and correct them to the rest frame of the GRB. For the two times (Tlag and TRT), the observed quantities must be divided by 1+z to correct for time dilation. The observed V value varies as the inverse of the time stretching, so our measured value must be multiplied by 1 + z to correct to the GRB rest frame. The observed Epeak value must be multiplied by 1 + z to correct for the redshift of the spectrum. The number of peaks in the light curve is defined in such a way as to have no z dependance. The dilation and redshift effects on thetajet and Egamma,iso have already been corrected in equations 1 and 2. A possibly substantial problem for the Tlag, V , and TRT relations is that we are in practice

limited to the available energy bands (c.f. Table 5) whereas these correspond to different energy bands in the GRB reference frame. Ideally, we would want to measure these indicators in observed energy bands that correspond to some consistent band in the GRB frame

1. Lag versus Luminosity ($T_{lag} - L$)
2. Variability versus Luminosity ($V - L$)
3. E_{peak} versus Luminosity ($E_{peak} - L$)
4. E_{peak} versus E_γ ($E_{peak} - E_\gamma$)
5. T_{RT} versus Luminosity ($T_{RT} - L$)
6. E_{peak} versus E_{iso} ($E_{peak} - E_{iso}$)

$$\log \frac{L}{\mathrm{erg\,s^{-1}}} = a_1 + b_1 \log \frac{\tau_{\mathrm{lag},i}}{0.1s}, \tag{1.2}$$

$$\log \frac{L}{\mathrm{erg\ s^{-1}}} = a_2 + b_2 \log \frac{V_i}{0.02}, \tag{1.3}$$

$$\log \frac{L}{\mathrm{erg\ s^{-1}}} = a_3 + b_3 \log \frac{E_{p,i}}{300\mathrm{keV}} \tag{1.4}$$

$$\log \frac{E_\gamma}{\mathrm{erg}} = a_4 + b_4 \log \frac{E_{p,i}}{300\mathrm{keV}}, \tag{1.5}$$

$$\log \frac{L}{\mathrm{erg\ s}} = a_5 + b_5 \log \frac{\tau_{\mathrm{RT},i}}{0.1\ \mathrm{s}}, \tag{1.6}$$

$$\log \frac{E_{\mathrm{iso}}}{\mathrm{erg}} = a_6 + b_6 \log \frac{E_{p,i}}{300\mathrm{keV}} \tag{1.7}$$

Assuming that GRBs radiate isotropically, the isotropic equivalent luminosity can be derived from the bolometric peak flux P_{bolo} by (Schaefer 2007)

$$L = 4\pi d_L^2 P_{\mathrm{bolo}}\ ,$$

where d_L is the luminosity distance of GRB, which can be obtained from the reconstructed distance moduli of Pantheon presented in section B with the relation

$$\mu = 5 \log \frac{d_L}{\mathrm{Mpc}} + 25.$$

Hence, the uncertainty of L propagates from the uncertainties of P_{bolo} and d_L. The isotropic equivalent energy E_{iso} can be obtained from the bolometric fluence S_{bolo} by

$$E_{\mathrm{iso}} = 4\pi d_L^2 S_{\mathrm{bolo}}\ (1+z)^{-1},$$

the uncertainty of E_{iso} propagates from the uncertainties of S_{bolo} and d_L. If on the other hand, GRBs radiate in two symmetric beams, then we can define the collimation-corrected energy E_γ as

$$E_\gamma \equiv E_{\mathrm{iso}}\ F_{\mathrm{beam}}\ ,$$

Correlation	sample	N	a	a_err	b	b_err	σ	σ_{int}
$T_{lag} - L$	low-z	37	52.09	0.11	-0.78	0.16	0.51	0.09
	high-z	32	52.59	0.07	-0.65	0.12	0.22	0.09
	All-z	69	52.32	0.07	-0.76	0.11	0.47	0.06
$V - L$	low-z	47	52.1	0.25	0.65	0.37	0.93	0.14
	high-z	57	52.8	0.15	0.34	0.14	0.62	0.07
	All-z	104	52.38	0.14	0.6	0.15	0.76	0.07
$E_{peak} - L$	low-z	50	51.87	0.09	1.47	0.19	0.59	0.07
	high-z	66	52.48	0.06	1.15	0.15	0.3	0.06
	All-z	116	52.17	0.06	1.44	0.14	0.55	0.05
$E_{peak} - E_{\gamma}$	low-z	12	50.63	0.08	1.56	0.19	0.23	0.09
	high-z	12	50.74	0.14	1.17	0.43	0.39	0.14
	All-z	24	50.67	0.07	1.47	0.17	0.26	0.07
$T_{RT} - L$	low-z	39	52.69	0.13	-1.34	0.19	0.48	0.07
	high-z	40	52.86	0.08	-0.81	0.17	0.34	0.07
	All-z	79	52.77	0.08	-1.23	0.13	0.45	0.05
$E_{peak} - E_{iso}$	low-z	40	52.56	0.1	1.6	0.2	0.6	0.08
	high-z	61	53.0	0.06	1.27	0.14	0.38	0.04
	All-z	101	52.8	0.06	1.53	0.13	0.52	0.04

Table 1.1: A test caption

where $F_{\rm beam} \equiv 1 - \cos\theta_{\rm jet}$ is the beaming factor, $\theta_{\rm jet}$ is the jet opening angle. The uncertainty of E_{γ} propagates from the uncertainties of $E_{\rm iso\ and}$ $F_{\rm beam}$.

In order to test if the correlations discussed in the above section vary with redshift, we divide the GRB samples into two subsamples corresponding to the following redshift bins: the low-z sample ($z \leq 1.4$) which consists of 50 GRBs, and the high-z sample ($z > 1.4$) which consists of 66 GRBs. We investigate the redshift dependence of luminosity correlations for this two subsamples, as well as for the full GRBs sample. To fit the six luminosity correlations, we apply the D'Agostini's liklihood[11]

$$\mathcal{L}\left(\sigma_{\rm int}, a, b\right) \propto \prod_{i} \frac{1}{\sqrt{\sigma_{\rm int}^2 + \sigma_{yi}^2 + b^2\sigma_{xi}^2}} \times \exp\left[-\frac{\left(y_i - a - bx_i\right)^2}{2\left(\sigma_{\rm int}^2 + \sigma_{yi}^2 + b^2\sigma_{xi}^2\right)}\right]$$

For each correlation and each redshift bin, By maximizing this joint likelihood function, we can derive the best-fitting parameters a, b and the intrinsic scatter σ_{int}, where the intrinsic scatter σ_{int} denotes any other unknown errors except for the measurement errors. The results of the fits and the number of GRBs used in each fit are summarized in (1.1).

We perform a Markov Chain Monte Carlo analysis to calculate the posterior probability density function (PDF) of parameter space. We assume a flat prior on all the free parameters and limit $\sigma_{\rm int} > 0$. Note that not all GRBs can be used to analyze each luminosity correlation, because not all the necessary quantities are measurable for some GRBs. For example, GRBs without measurement of the spectrum lag can not used in the $\tau_{\rm lag} - L$ analysis. Hence, we present the best-fitting parameters, together with the number of available GRBs in each fitting in Table 1 In Figure 5 we plot all the six luminosity correlations in logarithmic coordinates. Low- z and high- z GRBs are represented by blue and red dots with the error bars denoting 1σ uncertainties. The blue line, red line and black line stand for the best-fitting results for low- z GRBs, high- z GRBs and all- z GRBs, respectively. The 1σ and 2σ contours and the PDFs for parameter space are plotted in Figure 6

As shown in Table 1 low- z GRBs have a smaller intercept, but a sharper slope than high- z

GRBs for all the six luminosity correlations. All- z GRBs have the parameter values between that of low- z and high- z subsamples. For the intrinsic scatter, low- z GRBs have larger value than high- z GRBs, and the $E_p - E_\gamma$ relation has the smallest intrinsic scatter hence we can only obtain its upper limit. The $V - L$ relation has the largest intrinsic scatter, thus it can not be fitted well with a simple line, which is legible in Figure [5 In Figure 6 the contours in the (a, b) plane indicate that the $E_p - E_\gamma$ relation of low- z GRBs is consistent with that of high- z GRBs at 1σ confidence level. For the rest luminosity correlations, however, the intercepts and slopes for low- z GRBs differ from that of high- z GRBs at more than 2σ confidence level.

1.5.3 Calibrating distance modulus from $E_{peak} - E_{gamma}$ relation

Having luminosity correlations calibrated, we can conversely using these correlations to calibrate the distance of GRBs, and further use GRBs to constrain cosmological models. Since our calibration of luminosity correlations is independent of cosmological model, the circularity problem is avoided. As we have seen, the $E_p - E_\gamma$ relation is not significantly evolving with redshift, so we use this relation to calibrate the distance of GRBs. Due to that the TABLE 1

1.5.4 Constraints on the dark energy

Luminosity distance can be written as

$$d_L = c(1+z)\int_0^z \frac{1}{H(z)}dz \tag{1.8}$$

For flat ΛCDM, $H(z)$ can be written as

$$H(z) = H_0\sqrt{\Omega_M(1+z)^2 + 1 - \Omega_M} \tag{1.9}$$

We use emcee[12] to fit the dark energy equation. With the Pantheon dataset, the matter density of the flat ΛCDM model is constrained to be $\Omega_M = 0.278 \pm 0.007$. With 24 long GRBs alone, the matter density is constrained to be $\Omega_M = 0.307 \pm 0.065$. It indicates that the Hubble diagram in high redshift is consistent with the ΛCDM model

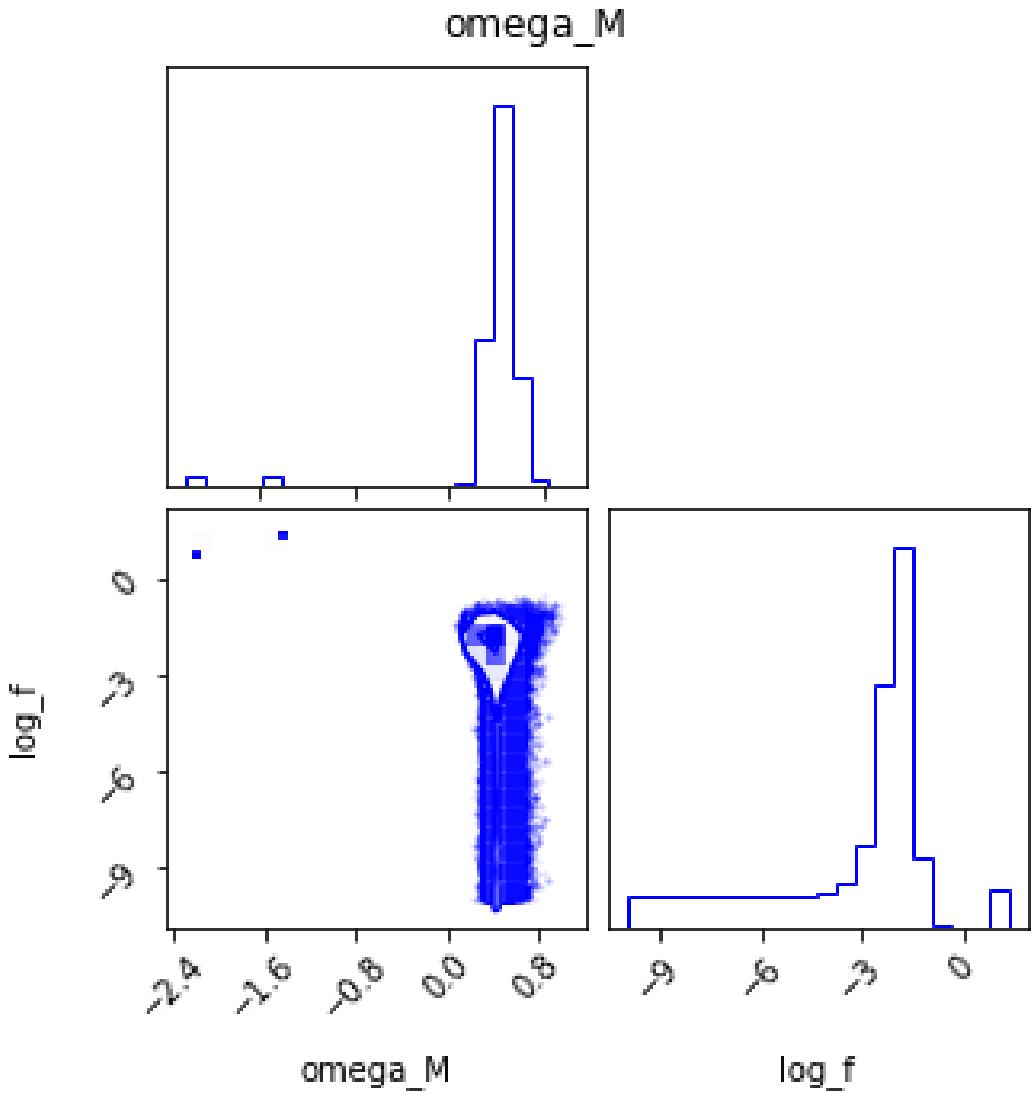

Figure 1.5: GRB Hubble Diagram

1.6 Reconstruction and calibration of distance modulus using Deep Learning

We construct the RNN+BNN network and train it with the package TensorFlow2[13]. For clarity, we present the corresponding hyperparameters in Figure 1 and list the steps to reconstruct data with our network as follow: (a) Data processing. The scale of data has an effect on training. Hence, we normalize the distance moduli of the sorted Pantheon data and re-arrange $\mu - z$ as sequences with the step number t = 4. (b) Building RNN. We build RNN with three layers, i.e. an input layer, a hidden layer and an output layer as described in Figure 1. The first two layers are constructed with the LSTM cells of 100 neurons. The redshifts $z_{<t>}$ and the corresponding distance moduli $\mu_{<t>}$ are the input and output vectors, respectively. We employ the Adam optimizer to minimize the cost

Correlation	sample	N	a	a_err	b	b_err	σ	σ_{int}
$T_{lag} - L$	low-z	37	52.1	0.1	-0.77	0.15	0.49	0.08
	high-z	32	52.37	0.07	-0.6	0.12	0.29	0.07
	All-z	69	52.22	0.06	-0.7	0.1	0.42	0.05
$V - L$	low-z	47	52.12	0.25	0.65	0.36	0.91	0.13
	high-z	57	52.63	0.18	0.25	0.17	0.63	0.07
	All-z	104	52.34	0.13	0.46	0.14	0.75	0.07
$E_{peak} - L$	low-z	50	51.89	0.09	1.43	0.18	0.59	0.07
	high-z	66	52.23	0.05	1.09	0.14	0.34	0.05
	All-z	116	52.05	0.05	1.35	0.12	0.5	0.04
$E_{peak} - E_{\gamma}$	low-z	12	50.66	0.09	1.47	0.2	0.25	0.09
	high-z	12	50.53	0.13	1.37	0.43	0.39	0.16
	All-z	24	50.61	0.06	1.45	0.16	0.25	0.07
$T_{RT} - L$	low-z	39	52.68	0.13	-1.3	0.19	0.48	0.07
	high-z	40	52.61	0.09	-0.74	0.17	0.39	0.06
	All-z	79	52.62	0.07	-1.08	0.12	0.44	0.04
$E_{peak} - E_{iso}$	low-z	40	52.57	0.1	1.55	0.2	0.6	0.08
	high-z	61	52.74	0.06	1.2	0.15	0.4	0.04
	All-z	101	52.65	0.05	1.42	0.12	0.49	0.04

Table 1.2: A test caption

function MSE and train the network 1000 times. (c) Building BNN. We set the dropout rate to 0 in the input layer to avoid the lost of information, and to 0.2 in the second layer as well as the output layer (Bonjean 2020; Mangena et al. 2020). We execute the trained network 1000 times to obtain the distribution of distance moduli

1.6.1 Training

We train the neural network using pantheon data. The pantheon data is split into train and test data in equal size randomly. 512 datapoints are used for training and remaiing for testing. The network architecture is described in previous section. We use meansquared error loss and adam optimizer, with early stopping technique to prevent overfitting. Dropout technique with $dropout_rate = 0.2$. The hyperparameters used are $batch_size = 10$, $learning_rate$ = 1e-3, $patience = 5$.

1.6.2 Testing redshift dependence of luminosity correlations

1.6.3 Calibrating distance modulus from $E_{peak} - E_{gamma}$ relation

1.6.4 Constraints on dark energy

1.7 Redoing analysis with Union Data

We redo all the analysis done for pantheon with union2.1 data and below are the results.

1.7.1 using Gaussian Processes

Training

The posterior drawn Gaussian process is shown below

Correlation	sample	N	a	a_err	b	b_err	σ	σ_{int}
$T_{lag} - L$	low-z	37	52.13	0.11	-0.79	0.16	0.53	0.08
	high-z	32	52.62	0.07	-0.65	0.12	0.36	0.06
	All-z	69	52.36	0.07	-0.77	0.11	0.5	0.05
$V - L$	low-z	47	52.11	0.25	0.65	0.37	0.93	0.14
	high-z	57	52.83	0.16	0.34	0.15	0.62	0.07
	All-z	104	52.4	0.14	0.6	0.15	0.76	0.07
$E_{peak} - L$	low-z	50	51.9	0.09	1.47	0.19	0.61	0.07
	high-z	66	52.52	0.06	1.13	0.15	0.41	0.04
	All-z	116	52.22	0.06	1.44	0.14	0.58	0.04
$E_{peak} - E_{\gamma}$	low-z	12	50.65	0.08	1.56	0.19	0.24	0.09
	high-z	12	50.76	0.14	1.18	0.42	0.4	0.14
	All-z	24	50.7	0.06	1.48	0.17	0.27	0.07
$T_{RT} - L$	low-z	39	52.71	0.13	-1.34	0.19	0.51	0.07
	high-z	40	52.9	0.08	-0.83	0.18	0.43	0.06
	All-z	79	52.8	0.08	-1.23	0.13	0.49	0.05
$E_{peak} - E_{iso}$	low-z	40	52.58	0.1	1.6	0.2	0.6	0.08
	high-z	61	53.03	0.06	1.28	0.14	0.39	0.04
	All-z	101	52.83	0.06	1.53	0.13	0.52	0.04

Table 1.3: A test caption

The error bars with predictions are shown belwo
Log Marginal Likelihood = -20.3
Score = 99.51

Testing redshift dependence of luminosity correlations

Calibrating distance modulus from $E_{peak} - E_{gamma}$ relation

Constraints on the dark energy

1.7.2 using Deep Learning

Training

Testing redshift dependence of luminosity correlations

Calibrating distance modulus from $E_{peak} - E_{gamma}$ relation

Constraints on dark energy

1.8 Conclusion

Correlation	sample	N	a	a_err	b	b_err	σ	σ_{int}
$T_{lag} - L$	low-z	37	52.14	0.1	-0.78	0.16	0.51	0.08
	high-z	32	52.18	0.08	-0.51	0.13	0.36	0.07
	All-z	69	52.14	0.06	-0.65	0.1	0.43	0.05
$V - L$	low-z	47	52.14	0.25	0.65	0.37	0.92	0.14
	high-z	57	52.56	0.24	0.1	0.23	0.66	0.07
	All-z	104	52.33	0.14	0.32	0.15	0.79	0.07
$E_{peak} - L$	low-z	50	51.92	0.09	1.46	0.18	0.6	0.07
	high-z	66	52.0	0.06	0.99	0.16	0.4	0.05
	All-z	116	51.95	0.05	1.28	0.12	0.5	0.04
$E_{peak} - E_{\gamma}$	low-z	12	50.67	0.08	1.56	0.18	0.21	0.08
	high-z	12	50.36	0.16	1.57	0.5	0.45	0.18
	All-z	24	50.54	0.07	1.58	0.17	0.28	0.08
$T_{RT} - L$	low-z	39	52.73	0.13	-1.33	0.19	0.48	0.07
	high-z	40	52.39	0.09	-0.63	0.18	0.43	0.06
	All-z	79	52.51	0.07	-0.98	0.12	0.46	0.05
$E_{peak} - E_{iso}$	low-z	40	52.6	0.1	1.6	0.2	0.59	0.08
	high-z	61	52.51	0.07	1.13	0.17	0.47	0.05
	All-z	101	52.53	0.06	1.36	0.13	0.52	0.04

Table 1.4: A test caption

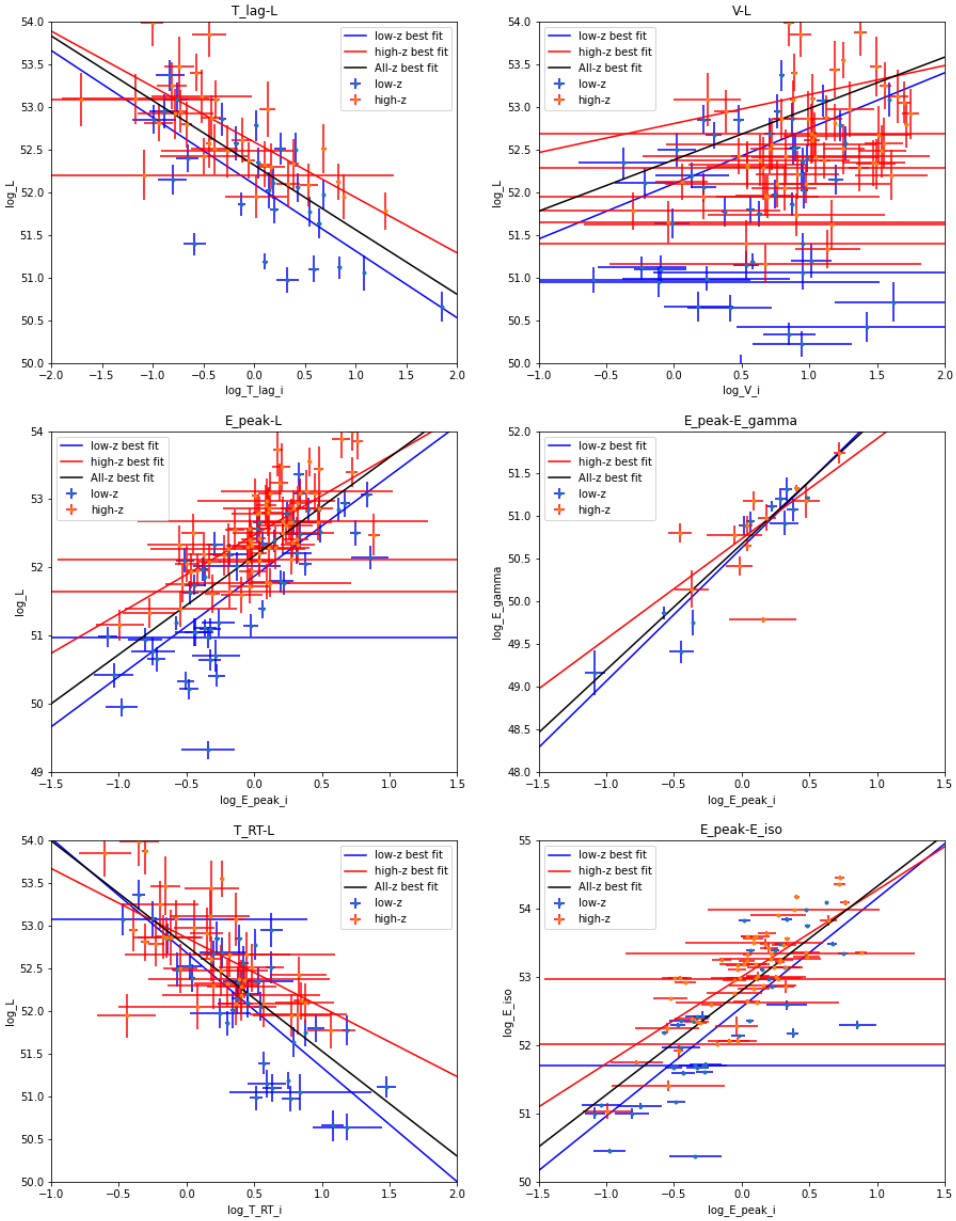

Figure 1.3: Luminsosity correlations best fit

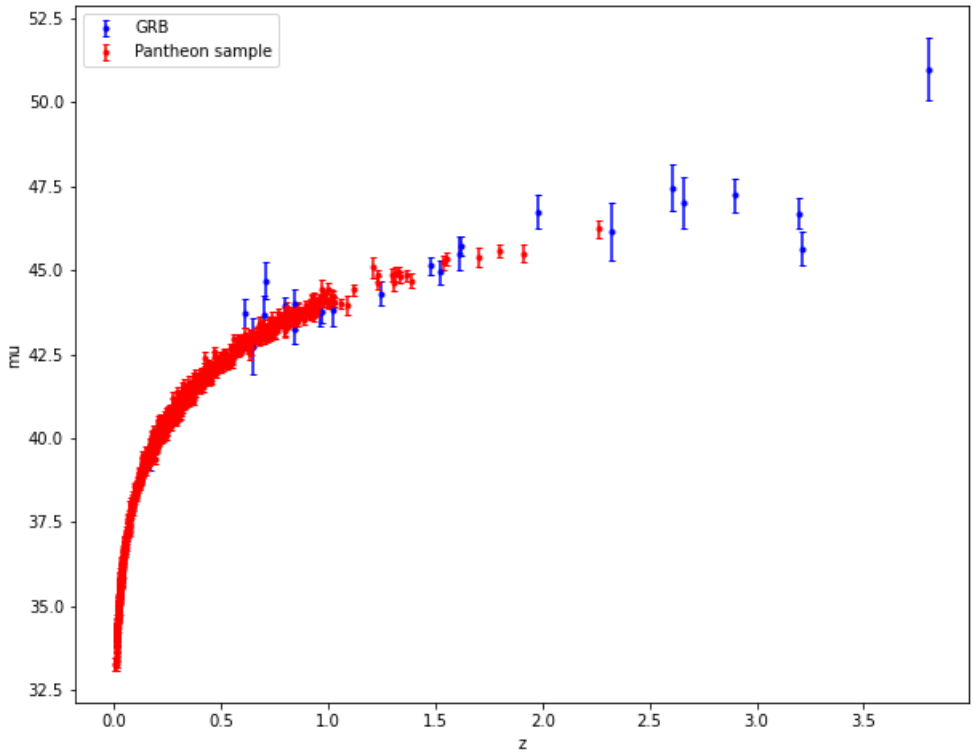

Figure 1.4: GRB Hubble Diagram

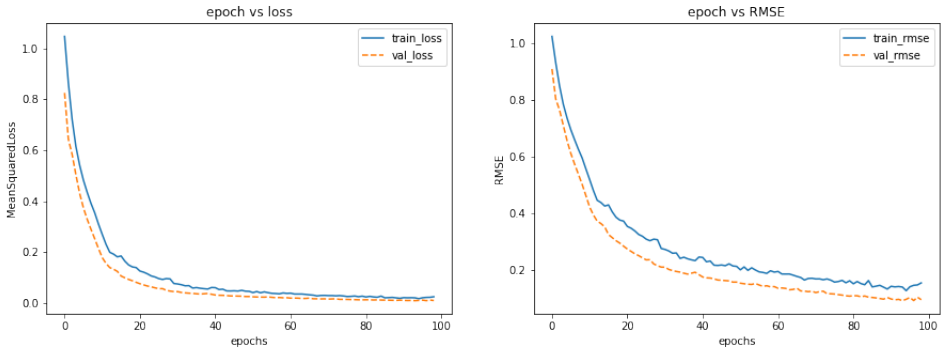

Figure 1.6: Loss curve

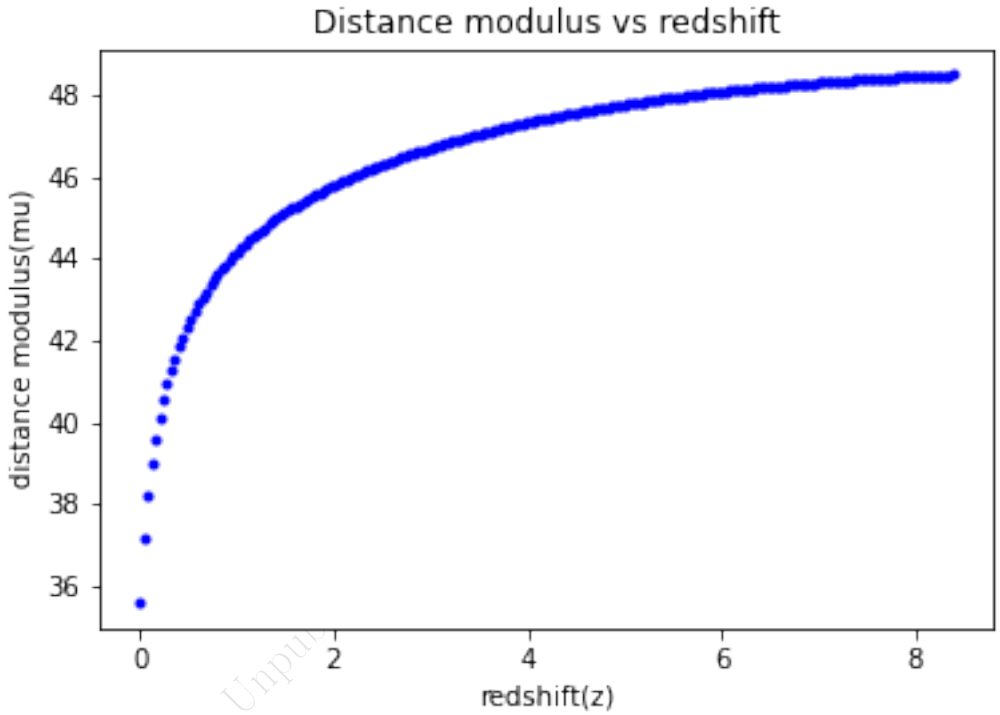

Figure 1.7: Loss curve

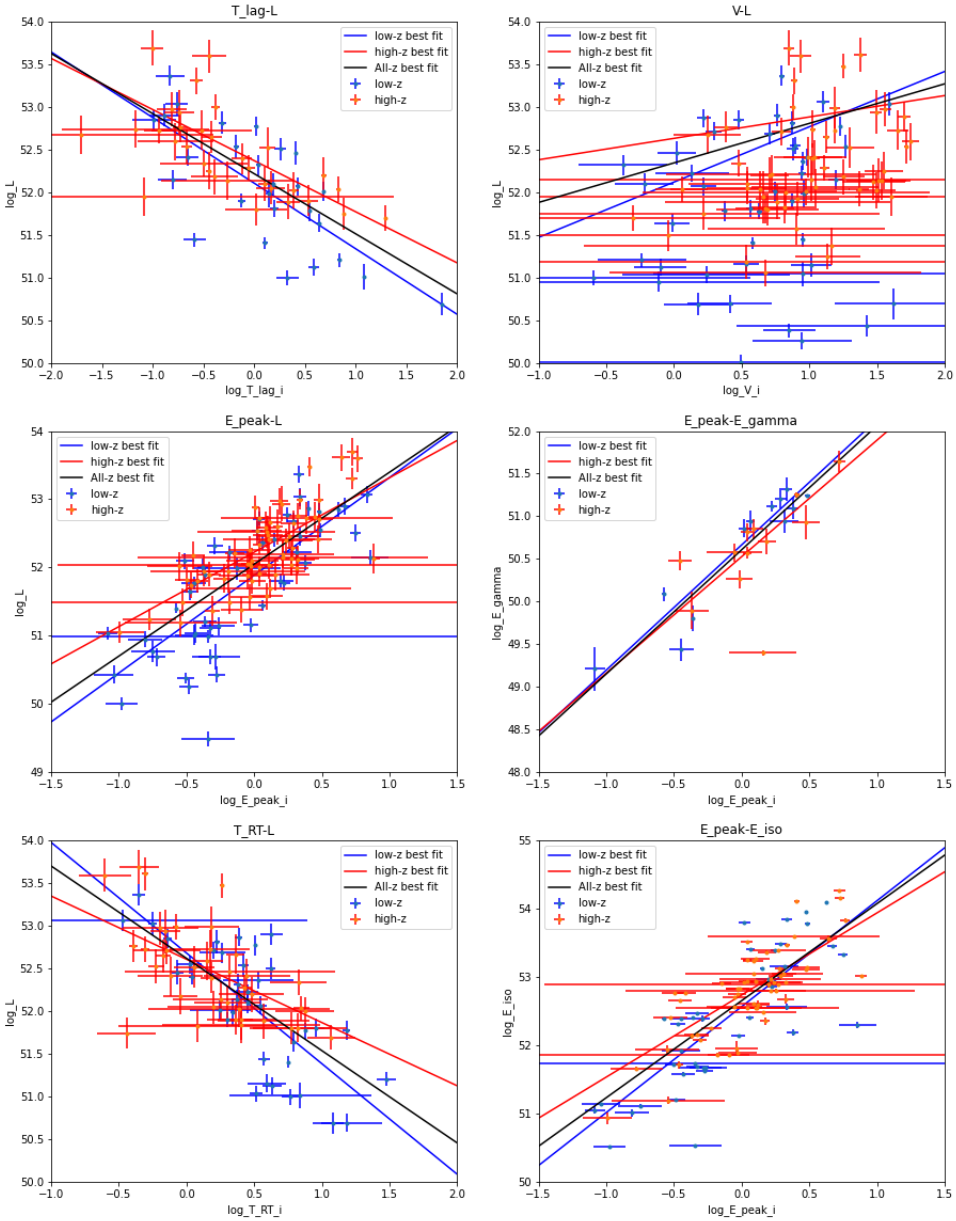

Figure 1.8: Luminsosity correlations best fit

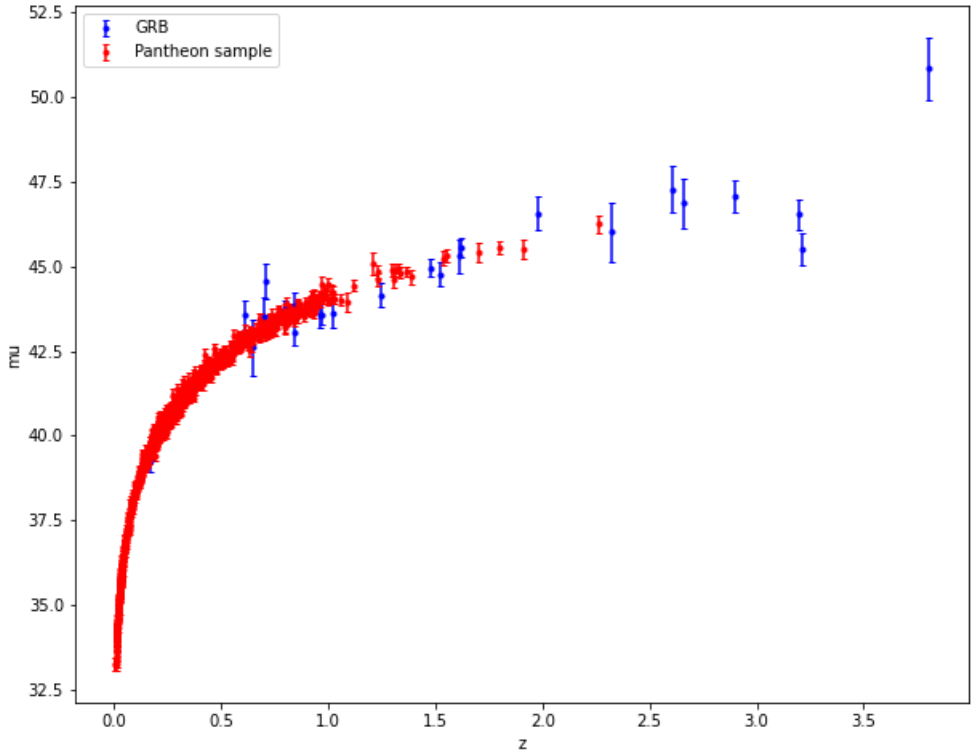

Figure 1.9: GRB Hubble Diagram

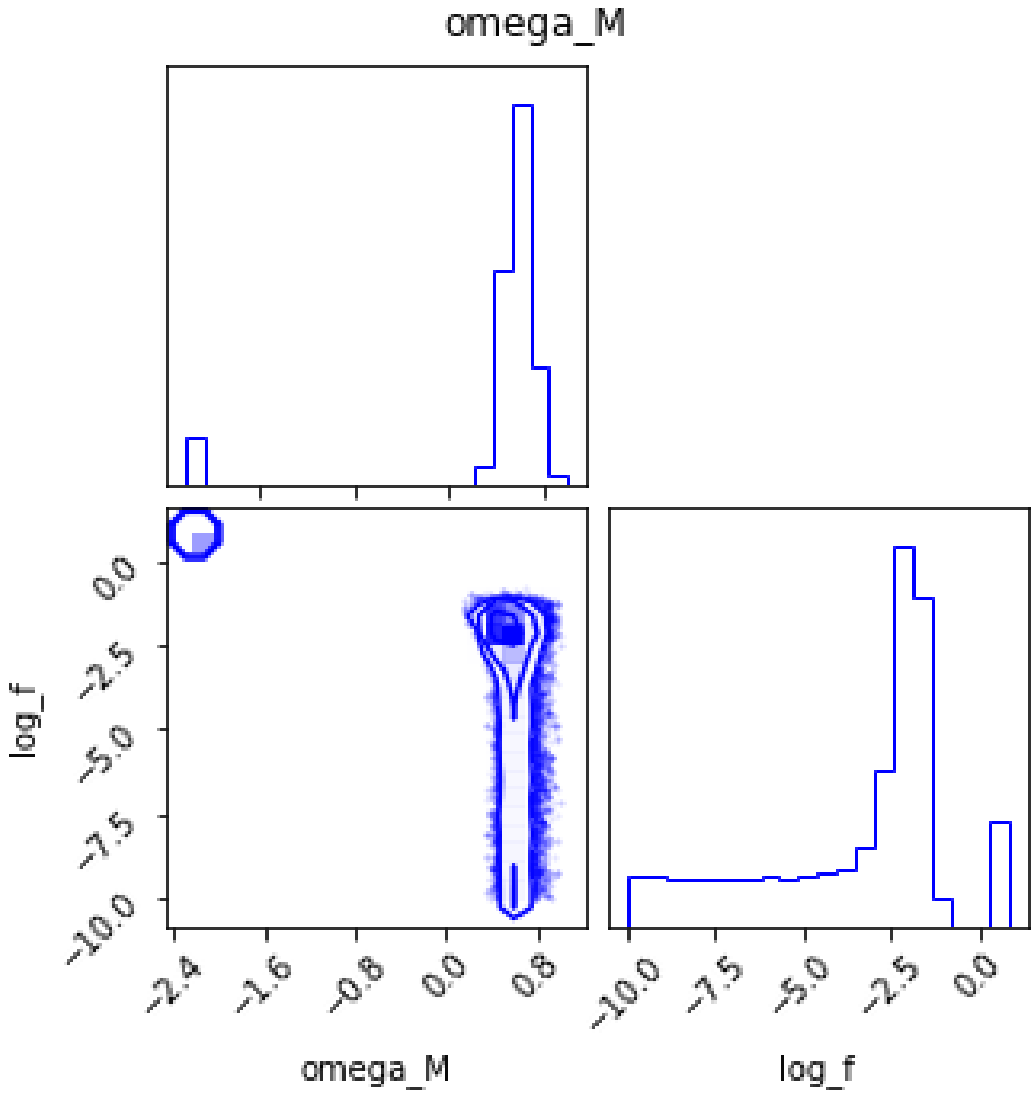

Figure 1.10: GRB Hubble Diagram

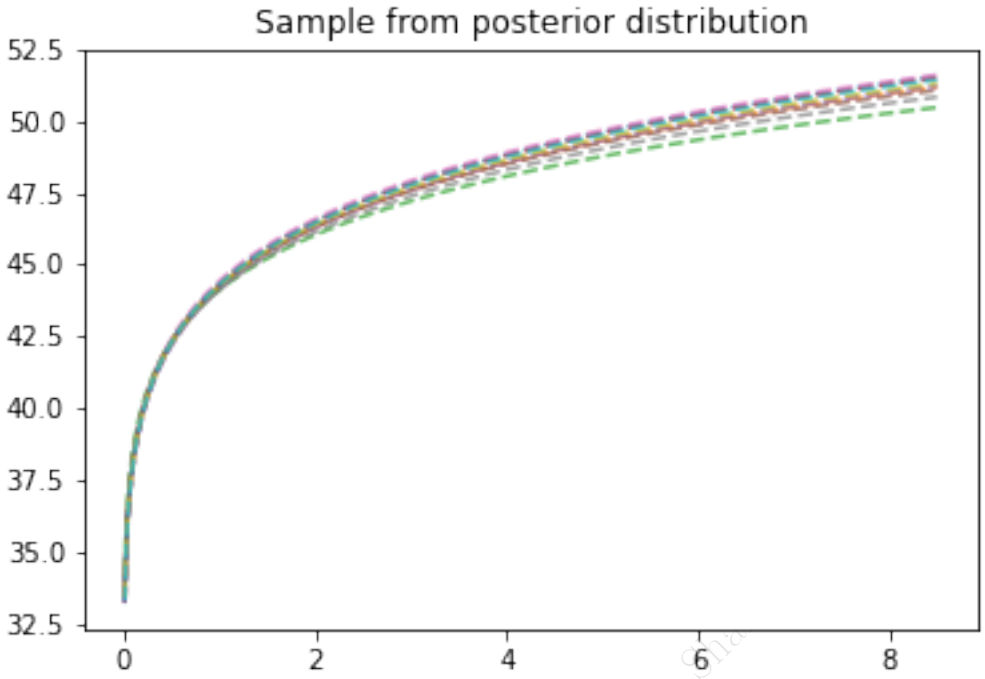

Figure 1.11: Posterior samples drawn from GP

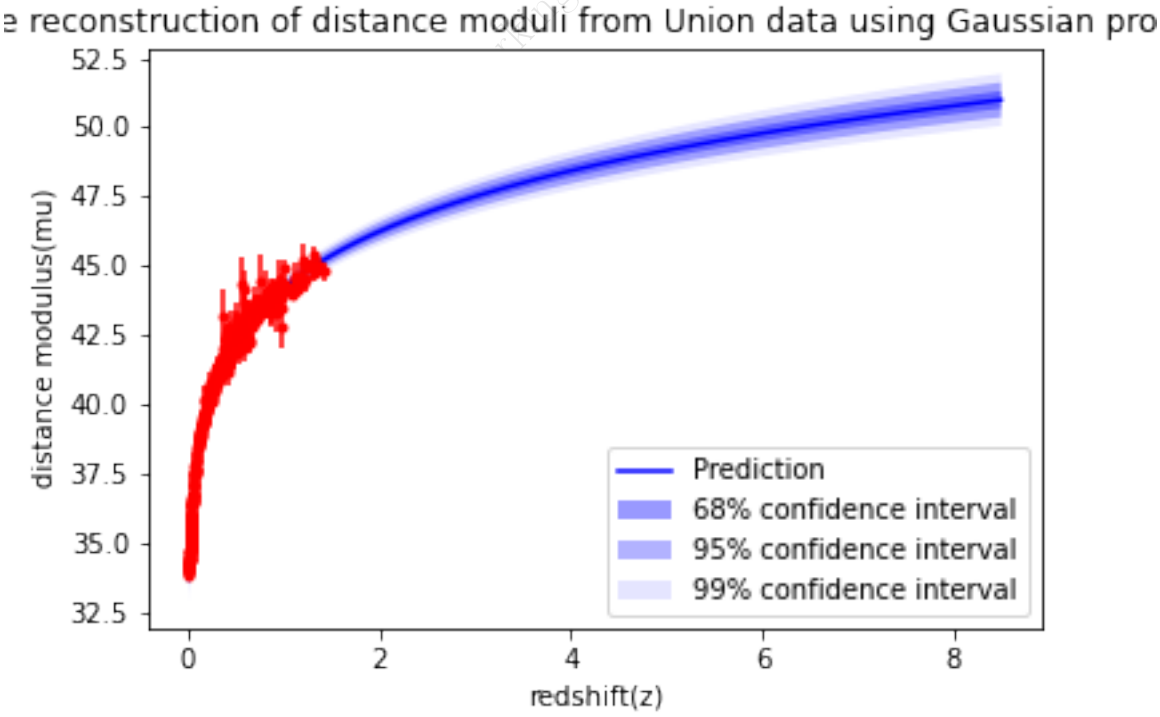

Figure 1.12: Reconstruction from Gaussian Processes

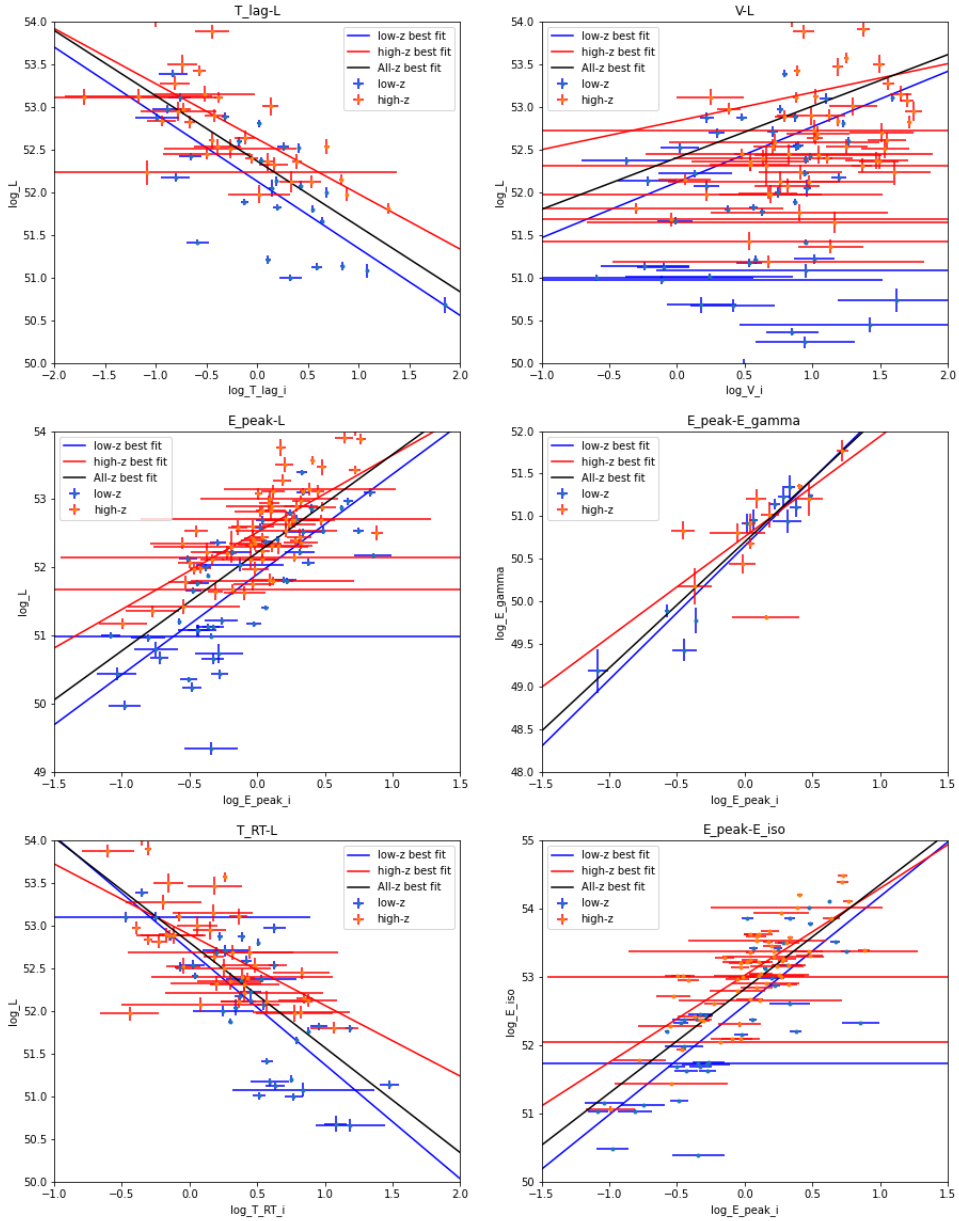

Figure 1.13: Luminsosity correlations best fit

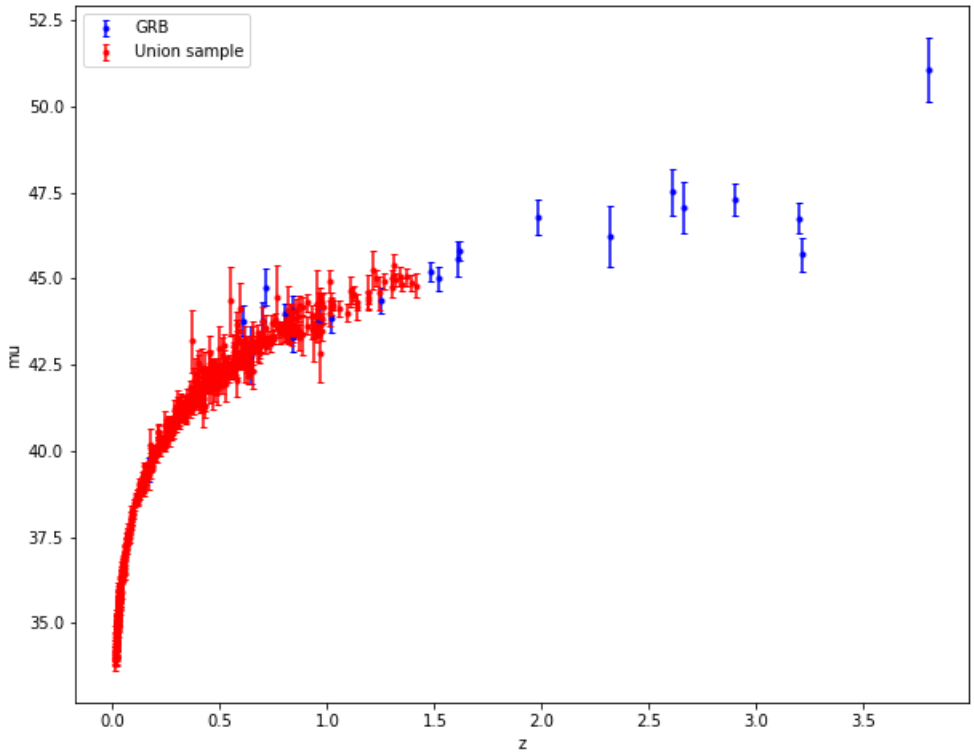

Figure 1.14: GRB Hubble Diagram

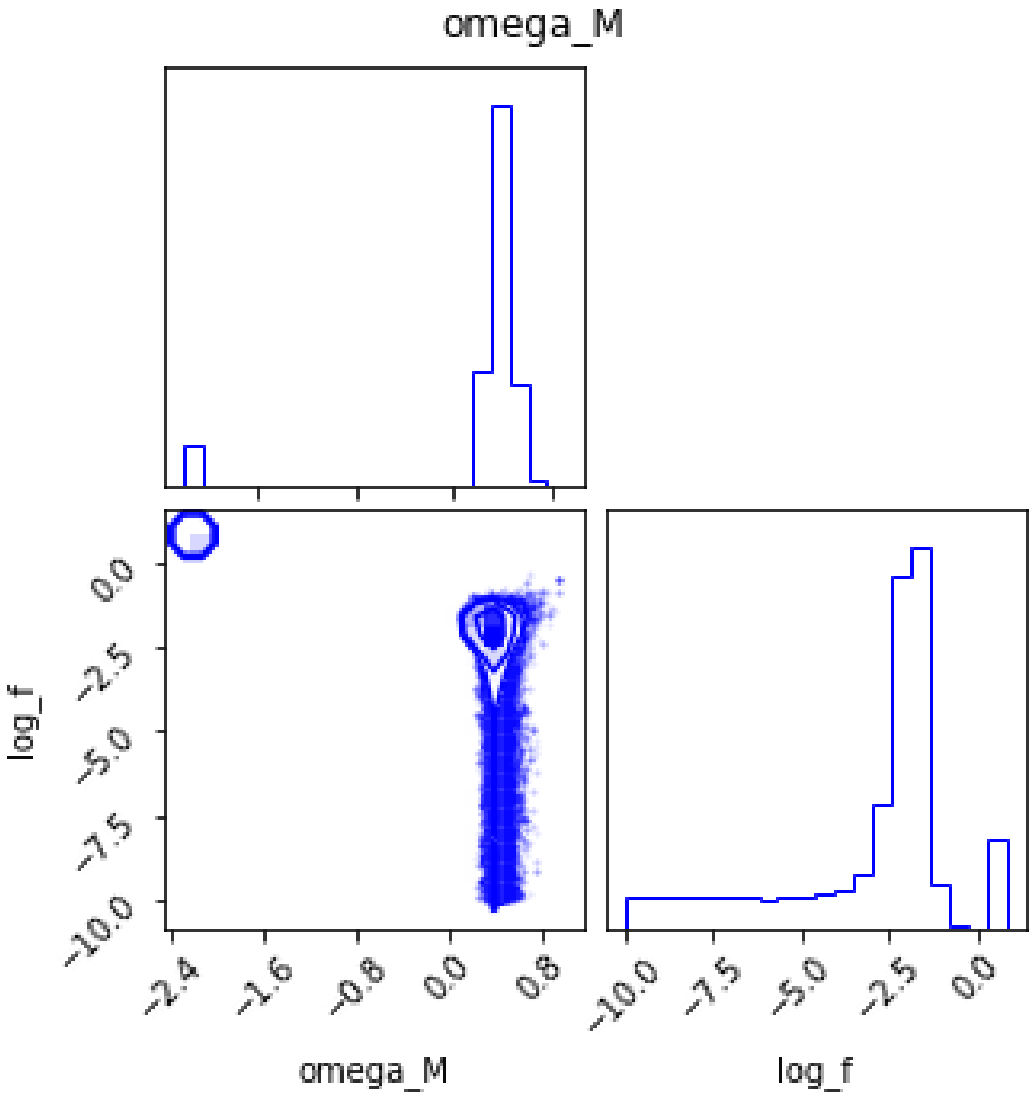

Figure 1.15: GRB Hubble Diagram

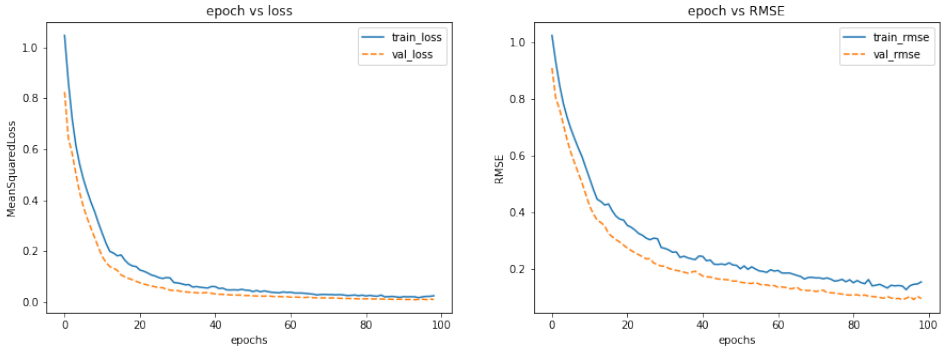

Figure 1.16: Loss curve

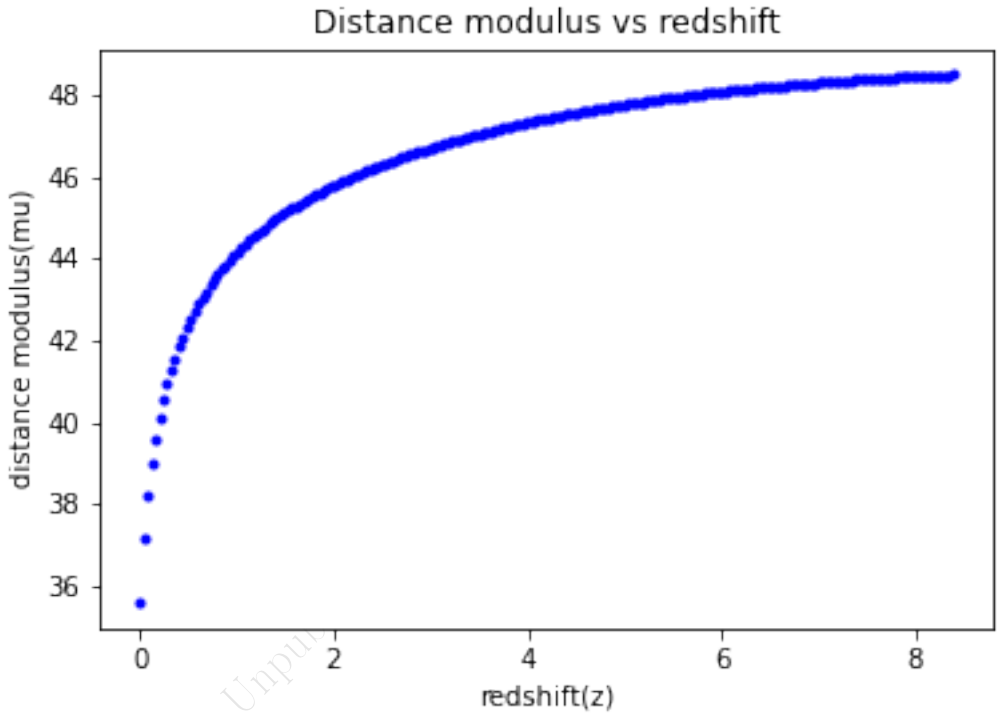

Figure 1.17: Loss curve

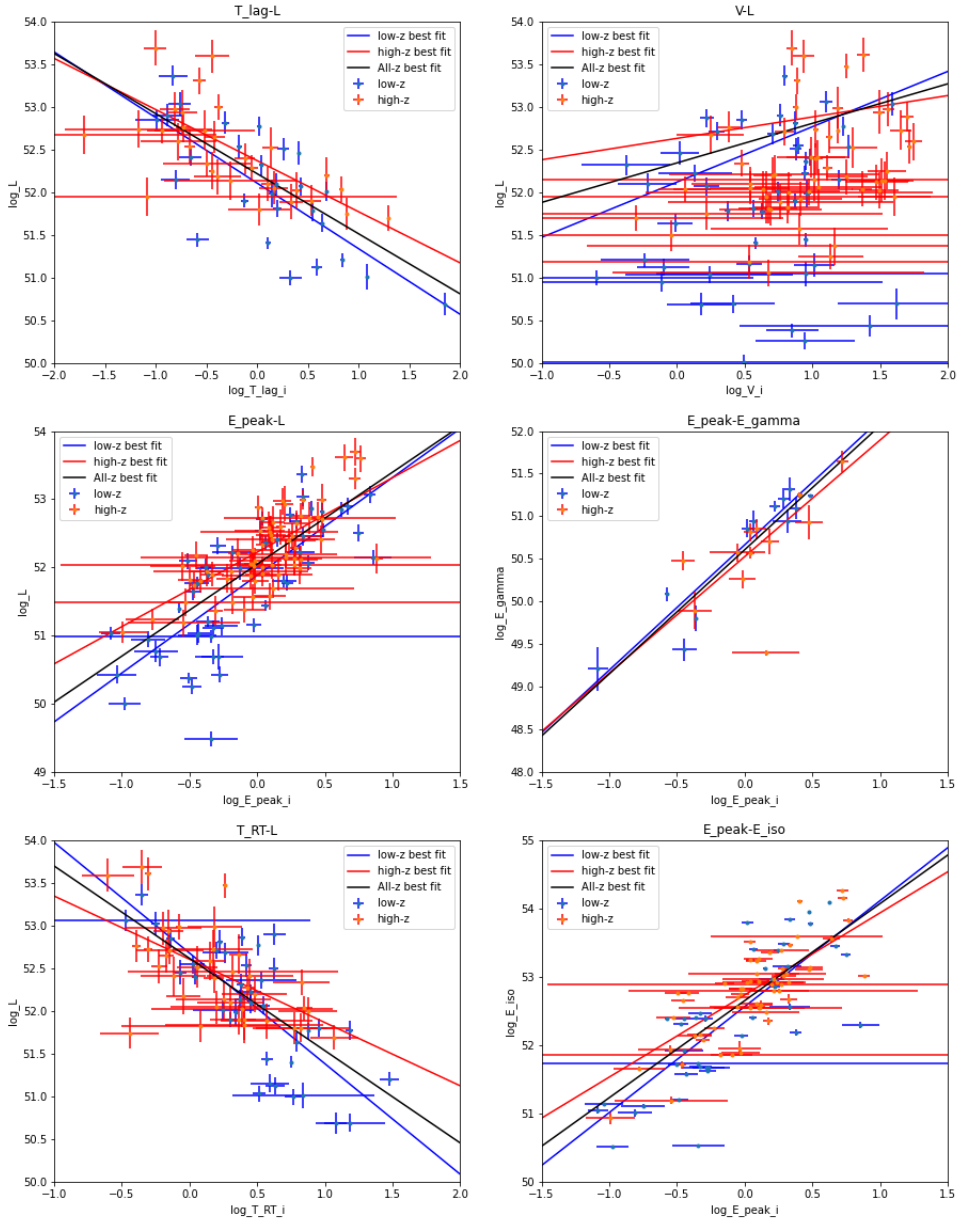

Figure 1.18: Luminsosity correlations best fit

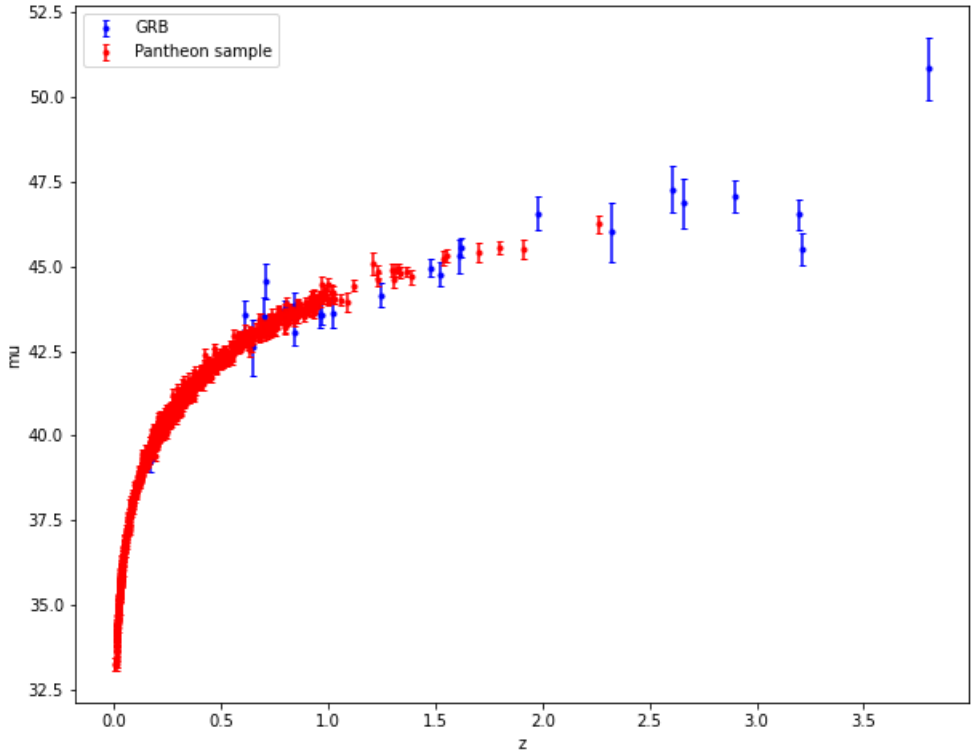

Figure 1.19: GRB Hubble Diagram

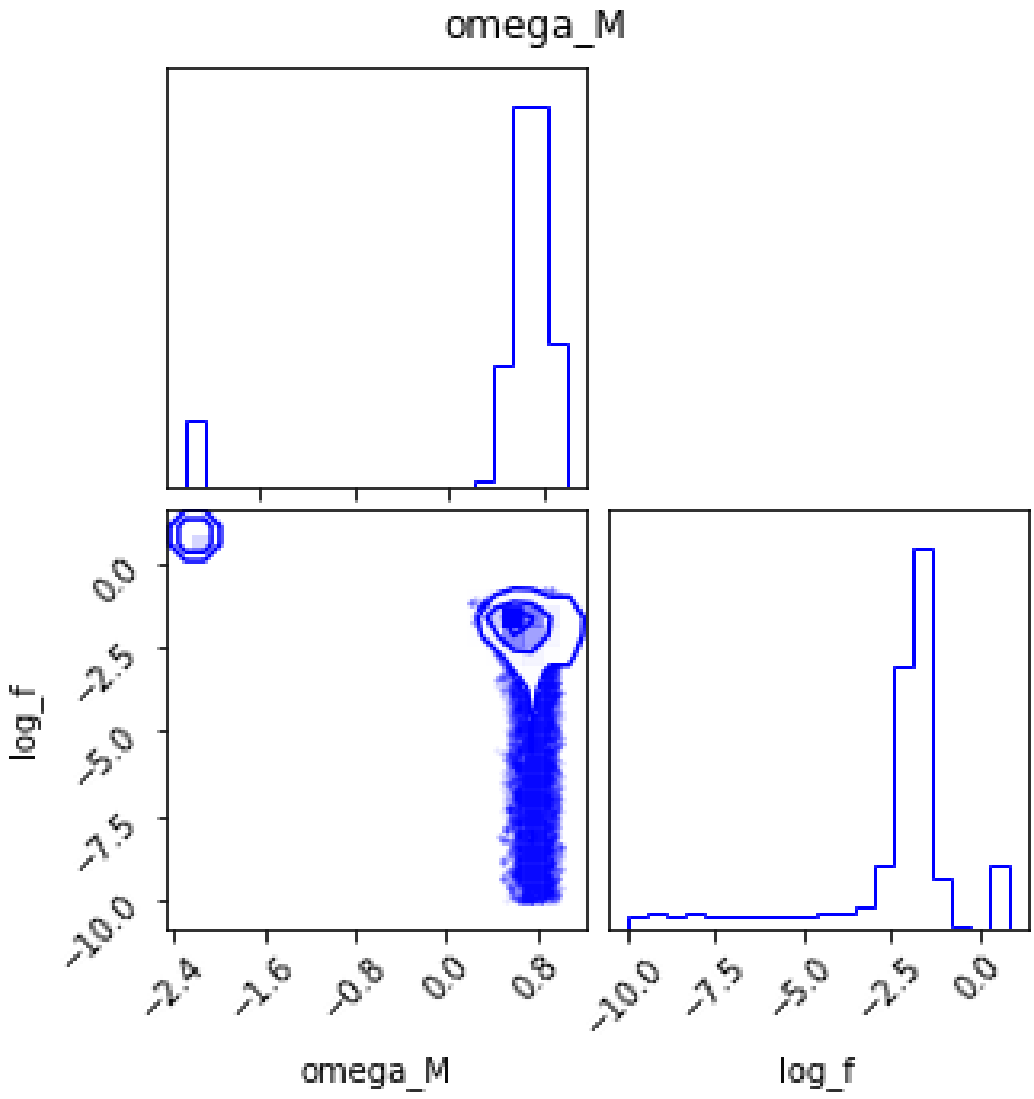

Figure 1.20: GRB Hubble Diagram

References

[1] A. G. Riess, A. V. Filippenko, P. Challis, A. Clocchiatti, A. Diercks, P. M. Garnavich, R. L. Gilliland, C. J. Hogan, S. Jha, R. P. Kirshner et al. Observational evidence from supernovae for an accelerating universe and a cosmological constant. *The Astronomical Journal* 116, (1998) 1009.

[2] S. Perlmutter, G. Aldering, G. Goldhaber, R. Knop, P. Nugent, P. G. Castro, S. Deustua, S. Fabbro, A. Goobar, D. E. Groom et al. Measurements of Ω and Λ from 42 high-redshift supernovae. *The Astrophysical Journal* 517, (1999) 565.

[3] B. E. Schaefer. The Hubble diagram to redshift$>$ 6 from 69 gamma-ray bursts. *The Astrophysical Journal* 660, (2007) 16.

[4] L.-X. Li. Variation of the Amati relation with cosmological redshift: a selection effect or an evolution effect? *Monthly Notices of the Royal Astronomical Society: Letters* 379, (2007) L55–L59.

[5] S. Basilakos and L. Perivolaropoulos. Testing gamma-ray bursts as standard candles. *Monthly Notices of the Royal Astronomical Society* 391, (2008) 411–419.

[6] F.-Y. Wang, S. Qi, and Z.-G. Dai. The updated luminosity correlations of gamma-ray bursts and cosmological implications. *Monthly Notices of the Royal Astronomical Society* 415, (2011) 3423–3433.

[7] L. Tang, X. Li, H.-N. Lin, and L. Liu. Model-independently calibrating the luminosity correlations of gamma-ray bursts using deep learning. *The Astrophysical Journal* 907, (2021) 121.

[8] D. M. Scolnic, D. Jones, A. Rest, Y. Pan, R. Chornock, R. Foley, M. Huber, R. Kessler, G. Narayan, A. Riess et al. The complete light-curve sample of spectroscopically confirmed SNe Ia from Pan-STARRS1 and cosmological constraints from the combined pantheon sample. *The Astrophysical Journal* 859, (2018) 101.

[9] N. Suzuki, D. Rubin, C. Lidman, G. Aldering, R. Amanullah, K. Barbary, L. Barrientos, J. Botyanszki, M. Brodwin, N. Connolly et al. The Hubble Space Telescope cluster supernova survey. V. Improving the dark-energy constraints above z$>$ 1 and building an early-type-hosted supernova sample. *The Astrophysical Journal* 746, (2012) 85.

[10] F. Pedregosa, G. Varoquaux, A. Gramfort, V. Michel, B. Thirion, O. Grisel, M. Blondel, P. Prettenhofer, R. Weiss, V. Dubourg, J. Vanderplas, A. Passos, D. Cournapeau, M. Brucher, M. Per-

rot, and E. Duchesnay. Scikit-learn: Machine Learning in Python. *Journal of Machine Learning Research* 12, (2011) 2825–2830.

[11] G. D'Agostini. Fits, and especially linear fits, with errors on both axes, extra variance of the data points and other complications. *arXiv preprint physics/0511182* .

[12] D. Foreman-Mackey, D. W. Hogg, D. Lang, and J. Goodman. emcee: The MCMC Hammer. *PASP* 125, (2013) 306–312.

[13] M. Abadi, A. Agarwal, P. Barham, E. Brevdo, Z. Chen, C. Citro, G. S. Corrado, A. Davis, J. Dean, M. Devin, S. Ghemawat, I. Goodfellow, A. Harp, G. Irving, M. Isard, Y. Jia, R. Jozefowicz, L. Kaiser, M. Kudlur, J. Levenberg, D. Mané, R. Monga, S. Moore, D. Murray, C. Olah, M. Schuster, J. Shlens, B. Steiner, I. Sutskever, K. Talwar, P. Tucker, V. Vanhoucke, V. Vasudevan, F. Viégas, O. Vinyals, P. Warden, M. Wattenberg, M. Wicke, Y. Yu, and X. Zheng. TensorFlow: Large-Scale Machine Learning on Heterogeneous Systems 2015. Software available from tensorflow.org.

Chapter 2

Model Comparison of Dark Energy models Using Deep Network

2.1 Introduction

2.2 Literature Survey

2.3 Observational Data

2.3.1 Union2.1

2.4 Methodology

2.4.1 VAE

2.4.2 GAN

2.4.3 VAEGAN

2.5 Test on toy model

2.6 Dark enrgy models

2.7 Conclusion

References

[1] A. G. Riess, A. V. Filippenko, P. Challis, A. Clocchiatti, A. Diercks, P. M. Garnavich, R. L. Gilliland, C. J. Hogan, S. Jha, R. P. Kirshner et al. Observational evidence from supernovae for an accelerating universe and a cosmological constant. *The Astronomical Journal* 116, (1998) 1009.

[2] S. Perlmutter, G. Aldering, G. Goldhaber, R. Knop, P. Nugent, P. G. Castro, S. Deustua, S. Fabbro, A. Goobar, D. E. Groom et al. Measurements of Ω and Λ from 42 high-redshift supernovae. *The Astrophysical Journal* 517, (1999) 565.

[3] B. E. Schaefer. The Hubble diagram to redshift$>$ 6 from 69 gamma-ray bursts. *The Astrophysical Journal* 660, (2007) 16.

[4] L.-X. Li. Variation of the Amati relation with cosmological redshift: a selection effect or an evolution effect? *Monthly Notices of the Royal Astronomical Society: Letters* 379, (2007) L55–L59.

[5] S. Basilakos and L. Perivolaropoulos. Testing gamma-ray bursts as standard candles. *Monthly Notices of the Royal Astronomical Society* 391, (2008) 411–419.

[6] F.-Y. Wang, S. Qi, and Z.-G. Dai. The updated luminosity correlations of gamma-ray bursts and cosmological implications. *Monthly Notices of the Royal Astronomical Society* 415, (2011) 3423–3433.

[7] L. Tang, X. Li, H.-N. Lin, and L. Liu. Model-independently calibrating the luminosity correlations of gamma-ray bursts using deep learning. *The Astrophysical Journal* 907, (2021) 121.

[8] D. M. Scolnic, D. Jones, A. Rest, Y. Pan, R. Chornock, R. Foley, M. Huber, R. Kessler, G. Narayan, A. Riess et al. The complete light-curve sample of spectroscopically confirmed SNe Ia from Pan-STARRS1 and cosmological constraints from the combined pantheon sample. *The Astrophysical Journal* 859, (2018) 101.

[9] N. Suzuki, D. Rubin, C. Lidman, G. Aldering, R. Amanullah, K. Barbary, L. Barrientos, J. Botyanszki, M. Brodwin, N. Connolly et al. The Hubble Space Telescope cluster supernova survey. V. Improving the dark-energy constraints above z$>$ 1 and building an early-type-hosted supernova sample. *The Astrophysical Journal* 746, (2012) 85.

[10] F. Pedregosa, G. Varoquaux, A. Gramfort, V. Michel, B. Thirion, O. Grisel, M. Blondel, P. Prettenhofer, R. Weiss, V. Dubourg, J. Vanderplas, A. Passos, D. Cournapeau, M. Brucher, M. Per-

rot, and E. Duchesnay. Scikit-learn: Machine Learning in Python. *Journal of Machine Learning Research* 12, (2011) 2825–2830.

[11] G. D'Agostini. Fits, and especially linear fits, with errors on both axes, extra variance of the data points and other complications. *arXiv preprint physics/0511182* .

[12] D. Foreman-Mackey, D. W. Hogg, D. Lang, and J. Goodman. emcee: The MCMC Hammer. *PASP* 125, (2013) 306–312.

[13] M. Abadi, A. Agarwal, P. Barham, E. Brevdo, Z. Chen, C. Citro, G. S. Corrado, A. Davis, J. Dean, M. Devin, S. Ghemawat, I. Goodfellow, A. Harp, G. Irving, M. Isard, Y. Jia, R. Jozefowicz, L. Kaiser, M. Kudlur, J. Levenberg, D. Mané, R. Monga, S. Moore, D. Murray, C. Olah, M. Schuster, J. Shlens, B. Steiner, I. Sutskever, K. Talwar, P. Tucker, V. Vanhoucke, V. Vasudevan, F. Viégas, O. Vinyals, P. Warden, M. Wattenberg, M. Wicke, Y. Yu, and X. Zheng. TensorFlow: Large-Scale Machine Learning on Heterogeneous Systems 2015. Software available from tensorflow.org.

Chapter 3

Photometric redshift estimation using Symbolic Regression

References

[1] A. G. Riess, A. V. Filippenko, P. Challis, A. Clocchiatti, A. Diercks, P. M. Garnavich, R. L. Gilliland, C. J. Hogan, S. Jha, R. P. Kirshner et al. Observational evidence from supernovae for an accelerating universe and a cosmological constant. *The Astronomical Journal* 116, (1998) 1009.

[2] S. Perlmutter, G. Aldering, G. Goldhaber, R. Knop, P. Nugent, P. G. Castro, S. Deustua, S. Fabbro, A. Goobar, D. E. Groom et al. Measurements of Ω and Λ from 42 high-redshift supernovae. *The Astrophysical Journal* 517, (1999) 565.

[3] B. E. Schaefer. The Hubble diagram to redshift$>$ 6 from 69 gamma-ray bursts. *The Astrophysical Journal* 660, (2007) 16.

[4] L.-X. Li. Variation of the Amati relation with cosmological redshift: a selection effect or an evolution effect? *Monthly Notices of the Royal Astronomical Society: Letters* 379, (2007) L55–L59.

[5] S. Basilakos and L. Perivolaropoulos. Testing gamma-ray bursts as standard candles. *Monthly Notices of the Royal Astronomical Society* 391, (2008) 411–419.

[6] F.-Y. Wang, S. Qi, and Z.-G. Dai. The updated luminosity correlations of gamma-ray bursts and cosmological implications. *Monthly Notices of the Royal Astronomical Society* 415, (2011) 3423–3433.

[7] L. Tang, X. Li, H.-N. Lin, and L. Liu. Model-independently calibrating the luminosity correlations of gamma-ray bursts using deep learning. *The Astrophysical Journal* 907, (2021) 121.

[8] D. M. Scolnic, D. Jones, A. Rest, Y. Pan, R. Chornock, R. Foley, M. Huber, R. Kessler, G. Narayan, A. Riess et al. The complete light-curve sample of spectroscopically confirmed SNe Ia from Pan-STARRS1 and cosmological constraints from the combined pantheon sample. *The Astrophysical Journal* 859, (2018) 101.

[9] N. Suzuki, D. Rubin, C. Lidman, G. Aldering, R. Amanullah, K. Barbary, L. Barrientos, J. Botyanszki, M. Brodwin, N. Connolly et al. The Hubble Space Telescope cluster supernova survey. V. Improving the dark-energy constraints above z$>$ 1 and building an early-type-hosted supernova sample. *The Astrophysical Journal* 746, (2012) 85.

[10] F. Pedregosa, G. Varoquaux, A. Gramfort, V. Michel, B. Thirion, O. Grisel, M. Blondel, P. Prettenhofer, R. Weiss, V. Dubourg, J. Vanderplas, A. Passos, D. Cournapeau, M. Brucher, M. Per-

rot, and E. Duchesnay. Scikit-learn: Machine Learning in Python. *Journal of Machine Learning Research* 12, (2011) 2825–2830.

[11] G. D'Agostini. Fits, and especially linear fits, with errors on both axes, extra variance of the data points and other complications. *arXiv preprint physics/0511182* .

[12] D. Foreman-Mackey, D. W. Hogg, D. Lang, and J. Goodman. emcee: The MCMC Hammer. *PASP* 125, (2013) 306–312.

[13] M. Abadi, A. Agarwal, P. Barham, E. Brevdo, Z. Chen, C. Citro, G. S. Corrado, A. Davis, J. Dean, M. Devin, S. Ghemawat, I. Goodfellow, A. Harp, G. Irving, M. Isard, Y. Jia, R. Jozefowicz, L. Kaiser, M. Kudlur, J. Levenberg, D. Mané, R. Monga, S. Moore, D. Murray, C. Olah, M. Schuster, J. Shlens, B. Steiner, I. Sutskever, K. Talwar, P. Tucker, V. Vanhoucke, V. Vasudevan, F. Viégas, O. Vinyals, P. Warden, M. Wattenberg, M. Wicke, Y. Yu, and X. Zheng. TensorFlow: Large-Scale Machine Learning on Heterogeneous Systems 2015. Software available from tensorflow.org.